Phyton-
International Journal of
Experimental Botany

Tech Science Press

http://doi.org/10.32604/phyton.2026.078884

ARTICLE

Aneuploidy-Induced Floral and Fertility Defects in *Hibiscus syriacus* Revealed by Cytogenetics and Integrative Trait Analysis: Implications for Chromosome Engineering in Ornamental Breeding

Yun-Jae Ahn[1,2,3], Moon-Seok Kang[2] and Ki-Byung Lim[2,3,4,*]

[1]Floriculture Research Division, National Institute of Horticultural & Herbal Science, Wanju, Republic of Korea
[2]Department of Horticultural Science, Kyungpook National University, Daegu, Republic of Korea
[3]Institute of Agricultural Science and Technology, Kyungpook National University, Daegu, Republic of Korea
[4]World Horti Center, Kyungpook National University, Sangju, Republic of Korea
*Corresponding Author: Ki-Byung Lim. Email: kblim@knu.ac.kr

Received: 09 January 2026; Accepted: 12 March 2026; Published: 28 April 2026

ABSTRACT: Artificial polyploidy induction is widely used in ornamental breeding but can yield aneuploidy derivatives that vary in developmental stability and breeding utility. In *Hibiscus syriacus* 'Blue Bird', *in vivo* colchicine and oryzalin treatments generated regenerated shoots in which genome-size shifts were detected by flow cytometry; among the candidate lines, a subset reached flowering maturity and was characterized in detail. These flowering aneuploids displayed diverse floral alterations, including reduced corolla size, altered pigmentation, and partial conversion of stamens into petaloid organs. Flow cytometry and somatic chromosome counts indicated aneuploid status (150–182 chromosomes). Pollen morphology was highly variable, with frequent malformations and broad size distributions, and Alexander staining and *in vitro* germination assays showed markedly reduced viability and germination relative to the control. Cytological observations of microsporogenesis revealed abnormal products such as polyads and unequal tetrads, indicating disruption during late meiotic and/or post-meiotic stages. Targeted expression analysis of two anthocyanin-pathway genes showed uniform downregulation of DFR, whereas F3′5′H responses varied among lines, providing a limited but consistent signal in line with the observed pigmentation changes. For downstream analyses, lines were grouped a priori by explicit reproductive and developmental criteria into intermediate and severe classes, with severe lines failing to reach full anthesis and showing complete male sterility. Multivariate analyses were used in an exploratory manner and described severity-associated patterns and coordinated co-variation among pigmentation, floral organ composition, and male fertility traits within the analysed lines. Collectively, these results are consistent with induced aneuploidy in *H. syriacus* being accompanied by coordinated floral and reproductive changes in the material examined here, and they support the use of early ploidy screening and targeted cytogenetic triage to guide selection in ornamental breeding programmes.

KEYWORDS: Aneuploidy; chromosome dosage imbalance; floral organ transformation; pollen viability; ornamental plant breeding; microsporogenesis

1 Introduction

Artificial polyploidy induction has been widely utilized in plant breeding as a chromosome engineering strategy to enhance desirable traits, including increased vigor, larger flowers, and improved stress tolerance [1]. Chemical chromosome doubling using agents such as colchicine and oryzalin has generated commercially valuable cultivars in ornamental crops like *Chrysanthemum*, *Impatiens*, *Lilium*,

and *Tulipa* [2–5]. However, these treatments can inadvertently produce aneuploids, defined as plants with irregular chromosome numbers arising from incomplete chromosome segregation or spindle disruption during mitosis [6,7]. Such unbalanced karyotypes disrupt dosage-sensitive developmental pathways, leading to metabolic imbalances and impaired organogenesis. Across species, unintended aneuploid plants have frequently exhibited pronounced developmental and reproductive defects, including markedly reduced fertility and altered floral morphology, without identifiable advantages in stress tolerance or ornamental performance [8–11].

Hibiscus syriacus L., commonly known as Rose of Sharon, is an ornamental shrub symbolically associated with Korea and valued worldwide for its prolific, colorful blooms [12–14]. Breeding programs target novel flower colors, double-petal forms, extended bloom periods, and improved stress resilience; however, progress is slowed by strong self-incompatibility and a long juvenile period, which restrict seed set and necessitate inter-varietal or interspecific crosses [12,15,16]. Within the genus *Hibiscus*, most studies have focused on transcriptomic profiles of individual cultivars [17,18] or comparisons between diploids and natural polyploids [14], with little attention to the developmental and reproductive consequences of unbalanced karyotypes [19]. Consequently, systematic analyses of artificially induced aneuploidy in *H. syriacus* that integrate cytogenetics, morphology, and fertility remain notably lacking.

In this study, we applied colchicine and oryzalin to *H. syriacus* 'Blue Bird' with the aim of inducing stable polyploids, but instead recovered a collection of aneuploid individuals. This unexpected outcome provided a rare opportunity to examine the multifaceted impacts of aneuploidy in an economically important ornamental species. We combined cytogenetic verification, detailed morphological and floral trait assessments, pollen viability and germination assays, and quantitative expression analysis of two key anthocyanin biosynthesis genes, DFR (dihydroflavonol 4-reductase) and F3′5′H (flavonoid 3′,5′-hydroxylase) [18,20], which are associated with the altered pigmentation patterns in the pink and white aneuploid flowers. By integrating cytology, phenotype, fertility, and molecular data, we clarify how chromosomal imbalance shapes *H. syriacus* development and reproduction and propose criteria for early recognition and discard of dosage-imbalanced genotypes, providing practical guidance for chromosome engineering-based ornamental *Hibiscus* breeding.

2 Materials and Methods

2.1 Antimitotic Treatment and Recovery of Aneuploid Lines

Cuttings from one-year-old *H. syriacus* 'Blue Bird' plants were rooted and grown in pots under greenhouse conditions at Kyungpook National University (25°C day/16°C night) until active shoot growth was established with 4–5 fully expanded leaves. Apical meristems of the rooted cuttings were then treated *in vivo* by applying 20 μL of colchicine or oryzalin solution across a predefined concentration series (see Table 1, for treatment outcomes) directly onto the shoot apical dome and the surrounding 2–3 young leaf primordia using a micropipette. The treatment was repeated every 24 h for three consecutive days. Each concentration treatment was applied to 25 plants. Newly emerged shoots from treated apices were subsequently propagated via cuttings for further analysis. All regenerated lines were screened for genome size variation by flow cytometry (Section 2.2), and lines with fluorescence peaks deviating from the control profile were retained for characterization, irrespective of whether full chromosome doubling was achieved.

Table 1: Recovery and screening outcomes in *H. syriacus* 'Blue Bird' following colchicine and oryzalin treatments across concentration series.

Treatments	Concentration	No. of Treated Cuttings	No. of Aneuploids	Aneuploid Recovery Rate (%)
Oryzalin	20 μM	25	7	28
	40 μM	25	6	24
	60 μM	25	2	8
	80 μM	25	3	12
Colchicine	0.05%	25	5	20
	0.1%	25	4	16
	0.2%	25	4	16
	0.5%	25	10	40

Aneuploid lines in this table refer to regenerated shoots showing genome-size shifts by flow cytometry relative to the control and retained for further evaluation.

2.2 Putative Ploidy Analysis Using Flow Cytometry

Relative genome size of all regenerated lines was estimated by flow cytometry prior to chromosome counting. Fresh leaf tissue (~1 cm^2) from each plant was coarsely chopped with a sterile razor blade in 500 μL of nuclei extraction buffer (Sysmex, Germany). The homogenate was filtered through a 30 μm nylon mesh into a 3 mL collection tube to remove cellular debris. The released nuclei were stained with staining buffer (Sysmex, Germany) according to the manufacturer's protocol. Fluorescence emission was measured using a Partec PA Ploidy Analyzer (Sysmex Partec GmbH, Germany), and genome size was determined from fluorescence peak positions relative to the control ('Blue Bird'). Lines showing fluorescence peaks deviating from the control profile were recorded as aneuploid candidates for subsequent cytological analysis. Of the 41 aneuploid lines initially recovered across all treatments, only eight (five pink- and three white-flowered) survived to maturity and were subsequently characterized in detail in this study.

2.3 Somatic Chromosome Preparation

Actively growing root tips (1–2 cm) were excised from potted plants and pretreated in 1 M α-bromonaphthalene at 20°C for 5 h to accumulate metaphase cells. Root tips were then fixed in Carnoy's solution (glacial acetic acid: absolute ethanol, 1:3, v/v) at room temperature overnight. For long-term storage, fixed material was transferred to 70% ethanol and kept at −20°C until use.

Prior to enzymatic digestion, root tips were rinsed in distilled water for 10–30 min and soaked in 0.1 M citrate buffer for 3 min. Cell walls were digested in an enzyme mixture containing 0.3% pectolyase Y-23, 0.3% cellulase RS, and 0.3% cytohelicase in 0.01 M citrate buffer at 37°C for 1 h. After digestion, the enzyme solution was removed, and 50 μL of Carnoy's solution was added. Samples were vortexed vigorously for 1–3 min until the suspension became cloudy, then centrifuged at 12,000 rpm for 3 min. The supernatant was discarded, and the pellet was resuspended in 25 μL of glacial acetic acid: absolute ethanol (9:1, v/v). The cell suspension was dropped onto ethanol-cleaned slides, steamed at 70°C for 10–15 s, and air-dried to prepare chromosome spreads. This slide preparation protocol was modified from [21]. For comparison with flow cytometry data, chromosome number of the control tetraploid (2n = 4x = 84) was set to 1.0, and relative chromosome numbers for each aneuploid line were calculated as (chromosome number of the line ÷ 84). These relative values were compared with relative DNA content obtained by flow cytometry.

2.4 Fluorescence In Situ Hybridization (FISH)

Fluorescence *in situ* hybridization was performed following the protocol of [22] with minor modifications. Slides were pre-treated with RNase A in 2× SSC buffer at 37°C for 60 min, rinsed three times in 2× SSC, and fixed in 4% paraformaldehyde for 10 min. The 45S and 5S rDNA probes were indirectly labeled with biotin-16-dUTP and digoxigenin-11-dUTP using a High Fidelity Biotin16 PCR Labeling Kit and a PCR DIG Probe Synthesis Kit, respectively. The hybridization mixture contained 50% deionized formamide, 1.25–2.50 ng·μL^{-1} of each probe, 2× SSC, and 10% dextran sulfate. This mixture was denatured at 70°C for 10 min before application to the slides, which were subsequently denatured at 80°C for 5 min and incubated in a humid chamber at 37°C for 16 h.

Following hybridization, slides were washed in 0.1× SSC at 42°C for 30 min. Digoxigenin and biotin signals were detected using FITC-conjugated anti-digoxigenin antibodies (Roche, Germany) and streptavidin Cy3 (Zymed Laboratories, USA), respectively. Chromosomes were counterstained with 1.5 μg·mL^{-1} DAPI (4′,6-diamidino-2-phenylindole) and observed under a fluorescence microscope (BX53, Olympus). Chromosome length measurements and karyotype analyses were performed using Cytovision software v7.4.

2.5 Morphological and Reproductive Phenotyping

Floral and vegetative traits were recorded from at least three flowering shoots per plant during peak blooming. Flower diameter, petal number, petal shape irregularities, and pigmentation patterns were documented using high-resolution photography and referenced to the RHS color chart (online version). Petal width was measured manually with a ruler, and bud morphology, style/stigma structure, and anther appearance were examined under a stereomicroscope (Olympus SZX16). Leaf length, width, and lamina shape were measured from fully expanded leaves collected from the third node of each plant. Phenotypes were categorized into “Normal”, “Intermediate”, and “Severe” groups based on floral morphology and pigmentation. For stomatal analysis, fully expanded leaves were sampled from each plant, and epidermal peels were prepared using the tape-peel method described by [23]. Peels were mounted on glass slides and observed under a light microscope (BX53, Olympus). Stomatal density (number of stomata per 100 μm^2) and guard cell length were measured from five randomly selected fields per sample (Table 2 and Supplementary Fig. S1).

Trichome characteristics were examined on the abaxial leaf surface under a stereomicroscope (Olympus SZX16). Leaf samples were observed directly without fixation or additional processing. Owing to the irregular morphology and high variability of trichomes in aneuploid plants, no quantitative measurements were taken; instead, representative images of tetraploid (control) and aneuploid individuals were captured to compare trichome density and structure qualitatively (Supplementary Fig. S1).

Table 2: Summary of floral and vegetative traits of control ('Blue Bird') and aneuploid *H. syriacus* lines. Measured traits include flower diameter, petal width, petal number, predominant petal color (RHS color chart code), number of stigmas, number of anthers, leaf length and width, stomatal length, guard cell width, and stomatal density. Chromosome numbers were determined from somatic spreads, with relative increases over the tetraploid control (2n = 4x = 84) shown as approximate ploidy levels in parentheses. Lines were classified into "Normal", "Intermediate", or "Severe" groups based on overall floral morphology and pigmentation.

Group	Samples	Flower Diameter (cm)	Petal Width (cm)	Petal Number	Predominant Petal RHS Colour	No. of Stigma	No. of Anthers	Leaf Length (cm)	Leaf Width (cm)	Stomatal Length (μm)	Guard Cell Width (μm)	Stomatal Density (no./100 μm²)	Chromosome Number (Ploidy Level)
Normal	Control ('Blue Bird')	10.9	4.3	5.0	RHS N155A (Pale blue-grey)	5	160	6.1	3.8	41.8	19.1	3.0	2n = 4x = 84
Intermediate	Pink-1	8.8	4.0	5.0	RHS 56C (Pale pink)	5	146	6.3	4.1	46.4	19.5	2.1	2n = 154 (≈1.8×)
	Pink-2	8.9	4.6	5.0	RHS 68B (Pale pinkish violet)	5	140	6.7	4.7	51.0	20.0	2.1	2n = 164 (≈1.9×)
	Pink-3	6.4	2.7	5.0	RHS 61A (Very pale pink)	5	140	6.2	4.3	55.7	20.5	2.1	2n = 182 (≈2.2×)
	Pink-4	6.4	3.5	5.0	RHS 56C (Pale pink)	2	48	6.5	4.9	59.4	20.9	2.1	2n = 157 (≈1.9×)
	Pink-5	6.2	2.4	5.0	RHS 68C (Pale lilac)	5	46	6.8	4.0	59.8	21.2	2.1	2n = 158 (≈1.9×)
Severe	White-1	1.6	1.5	7.7	RHS N155D (White)	0	40	6.4	4.5	44.6	19.9	2.1	2n = 150 (≈1.8×)
	White-2	1.7	1.5	10.7	RHS N155D (White)	0	60	6.0	3.9	45.7	20.3	2.1	2n = 150 (≈1.8×)
	White-3	1.4	1.5	12.3	RHS N155D (White)	5	40	6.0	3.8	46.0	19.5	2.2	2n = 150 (≈1.8×)

2.6 Microsporogenesis Observation

Cytological analysis of microsporogenesis was performed to examine meiotic outcomes in control and aneuploid lines. Floral buds at the tetrad stage were fixed in Carnoy's solution (ethanol:acetic acid = 3:1) and stored at −20°C. Anthers were squashed in 1% aceto-orcein and observed under a BX53 light microscope (Olympus, Japan). For each genotype, meiotic products were examined and classified as regular tetrads or abnormal polyads (≥5 microspores) with or without obvious size irregularities and micronuclei. Because configurations in aneuploid lines were highly variable and sample sizes were limited, meiotic outcomes were summarized qualitatively using representative images (Supplementary Fig. S3).

2.7 Pollen Assays

Fresh pollen grains were collected in the morning from at least three flowers per plant. For pollen size measurements, a minimum of 100 grains per plant were imaged under a light microscope (BX53, Olympus) at ×200 magnification, and diameters were measured using ImageJ v1.54. In lines where normally developed pollen grains were extremely rare, all available intact grains were measured.

Pollen viability was assessed using Alexander staining [24], in which viable grains stain red-purple and aborted grains green-blue or transparent. Approximately 200–450 grains per plant were scored to calculate the percentage of viable pollen.

For *in vitro* germination tests, freshly collected pollen was placed on slightly modified *in vitro* pollen germination medium from [25]. Briefly, the *in vitro* pollen germination medium consists of 20% sucrose, 0.01% H_3BO_3, 0.03% $Ca(NO_3)_2{\cdot}4H_2O$, 0.02% $MgSO_4{\cdot}7H_2O$, 0.005% KNO_3, 0.05% MnSO4 (pH 6.5 without agar) and incubated for 4 h at 25°C. Germination was scored under a light microscope, with pollen considered germinated when the pollen tube was clearly visible. Germination percentage was calculated from approximately 110–400 grains per plant.

2.8 Gene Expression Analysis by Quantitative RT-PCR

Petal tissues were collected at full anthesis from 'Blue Bird' (control) and a subset of aneuploid lines chosen to represent the phenotypic severity spectrum. Among the five pink-flowered aneuploids (Pink 1–5), only three lines (Pink 1–3) showing intermediate phenotypic alterations were selected for qRT-PCR analysis. All three white-flowered aneuploids (White 1–3), which exhibited the most severe morphological defects, were included as the "severe" group. Total RNA was extracted according to [26]. Briefly, 100–200 mg of frozen petal tissue was ground in liquid nitrogen, homogenized in TRIzol reagent, and subjected to chloroform extraction and isopropanol precipitation. To reduce polysaccharide contamination, RNA pellets were further purified with sodium acetate/ethanol washes before final resuspension in DEPC-treated water. RNA concentration and purity were assessed with a NanoDrop spectrophotometer (Thermo Fisher). cDNA was synthesized from 1 μg of total RNA using the HiSense™ cDNA Synthesis Master Mix (CellSafe, Republic of Korea) with oligo (dT) primers.

Gene-specific primers for DFR and F3′5′H were newly designed based on *H. syriacus* transcript sequences (NCBI Gene IDs: LOC120216676 and LOC120115295), respectively, with 18S rRNA used as the internal reference gene (Supplementary Table S1). qRT-PCR reactions were performed in triplicate for each sample using the HiSense™ QGreenBlue qPCR Master Mix (CellSafe, Republic of Korea) on a StepOnePlus Real-Time PCR system (Thermo Fisher Scientific, USA). Relative expression levels were calculated using the $2^{-\Delta\Delta Ct}$ method, log10-transformed for analysis, and averaged across three biological replicates per genotype. Statistical differences among genotypes were assessed using one-way ANOVA followed by Tukey's HSD test on ΔCt values.

2.9 Data Processing and Visualization

Pollen diameter distributions and the radar and correlation plots were generated in Python 3.12 using pandas, NumPy, matplotlib, seaborn, and SciPy (accessed in 2025). Principal component analysis (PCA) was conducted using scikit-learn (v 1.5).

Pollen size processing. For pollen diameter measurements (≥100 grains per plant), values outside ±2 SD of the plant-specific mean were flagged as statistical outliers using a predefined rule. In addition, grains exceeding 180 μm were labeled descriptively as "giant pollen" and highlighted separately in the swarm plot. Group means ± SD were overlaid. Importantly, pollen viability and germination were quantified independently of pollen-size screening, so the key fertility conclusions do not hinge on a small number of extreme-size grains.

Trait scaling and visualization. For the radar plot, phenotypic traits were min-max normalized to a 0–1 range and averaged by severity group (Normal, Intermediate, Severe) prior to plotting on polar coordinates. For correlation plots, predefined trait pairs were visualized with group-specific colors, and Pearson's correlation coefficients (or Spearman's ρ, when assumptions for Pearson's correlation were not met) were calculated with regression lines.

Definition of Non-anther organ proportion (NAOP, %). Non-anther organ proportion (NAOP, %) was calculated as:

$$NAOP\ (\%) = \frac{(Total\ \text{counted}\ number\ of\ floral\ organs\ -\ Number\ of\ anthers)}{Total\ counted\ number\ of\ floral\ organs} \times 100$$

where Total counted number of floral organs = number of sepals + number of petals + number of stigmas + number of anthers. NAOP summarizes overall shifts in floral organ composition with particular sensitivity to anther reduction and accompanying changes in other floral organs (including stigma degeneration).

Principal component analysis. For PCA, the quantitative traits (flower diameter, anther development, stigma development, pollen viability, pollen germination, pollen size, NAOP, and relative expression of DFR and F3′5′H) were standardized (mean-centered and scaled to unit variance) prior to decomposition. PCA scores and loadings were visualized as a biplot, with samples colored by severity group and variable loadings shown as vectors. A sensitivity check was performed by repeating PCA after excluding a borderline line to confirm that the major multivariate patterns were not driven by a single sample.

3 Results

To summarize the outcomes of the antimitotic treatments, Table 1 reports recovery and screening results across the colchicine and oryzalin concentration series. Across treatments, a subset of regenerated shoots showed genome-size shifts by flow cytometry and were retained as candidate aneuploid lines for downstream characterization. These treatment-level outcomes provide the experimental context for the phenotypic and cytological analyses described below.

3.1 Floral and Vegetative Divergence

Among 41 candidate aneuploid lines initially flagged by flow cytometry (genome-size shifts relative to the control), only eight plants (five pink- and three white-flowered) reached maturity and produced flowers. These individuals were therefore subjected to morphological, cytological, and molecular characterization. The pink-flowered aneuploid lines (Pink 1–5) displayed a range of alterations in floral morphology compared with the control 'Blue Bird' (Table 2 and Figs. 1 and 2). Across all pink lines, mean flower diameter was

reduced from approximately 10.9 cm in the control to 6.2–8.9 cm, petals often exhibited irregular shapes and narrowed laminae, and anthocyanin pigmentation was reduced in intensity and coverage. RHS color chart (online version) comparison indicated petals from aneuploid lines ranging from RHS 56C (pale pink) to RHS 68C (pale lilac) while the control 'Blue Bird' petal was RHS N155A (Pale blue-grey). The white-flowered aneuploid lines (White 1–3) presented the most severe alterations, with significant loss of visible anthocyanin pigmentation, markedly reduced flower size (from 10.9 cm in the control to 1.4–1.7 cm), and conspicuously shortened or malformed stamens and stigma. RHS color chart (online version) classification placed petals uniformly within RHS N155D for white. All lines classified as Severe failed to achieve full anthesis; the partially expanded corollas visible in Fig. 2 represent their maximum bloom stage, and prolonged observation confirmed that buds senesced and abscised without ever reaching a fully expanded floral form.

Figure 1: Floral phenotypes of control and aneuploid lines. Whole-flower, petal, and bud phenotypes of (**A**) *H. syriacus* 'Blue Bird' (control) and (**B**–**I**) representative aneuploids (pink and white groups). Scale bars = 1 cm.

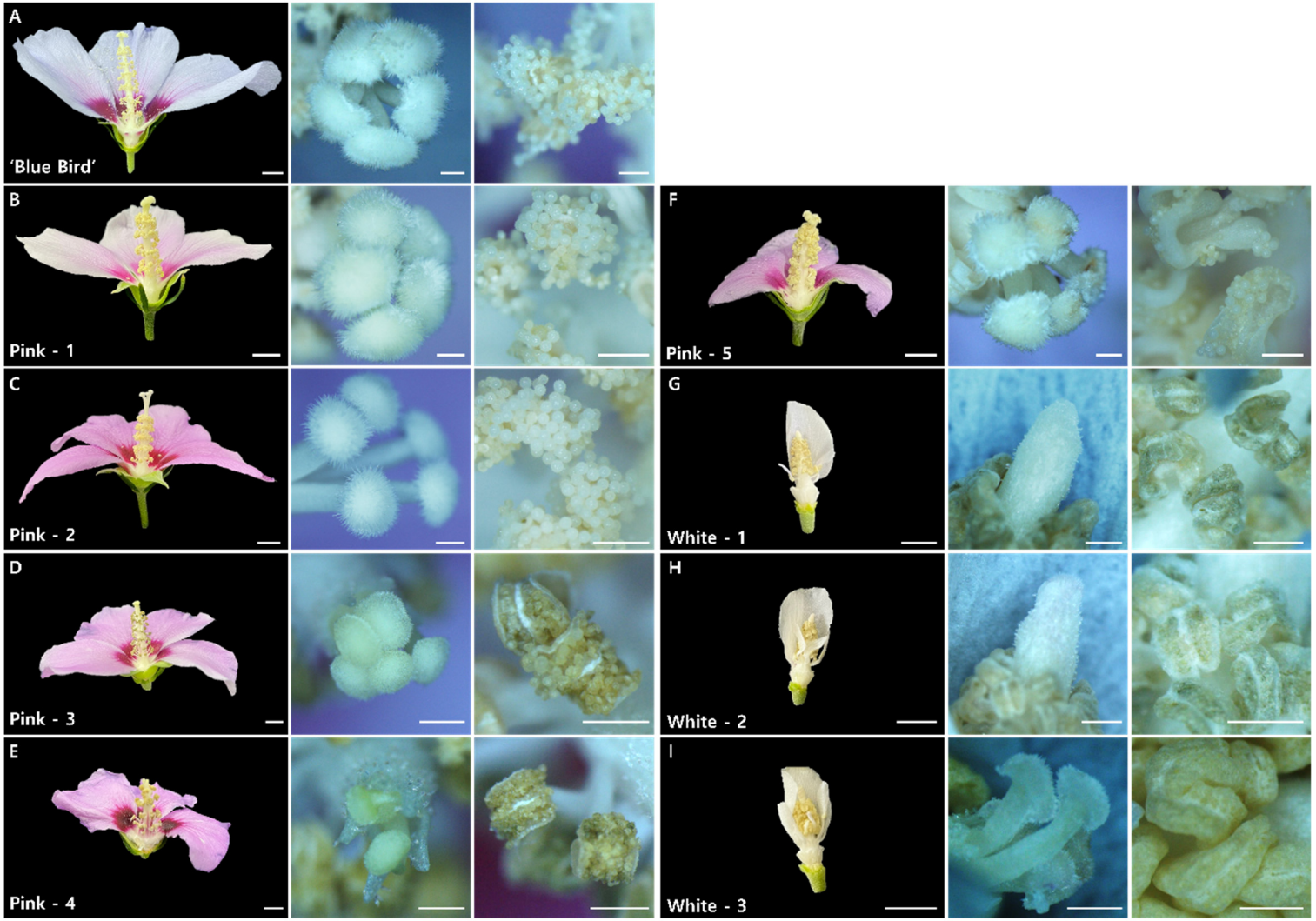

Figure 2: Reproductive organ morphology in control and aneuploid *H. syriacus*. (**A**) Longitudinal section of a flower from the control 'Blue Bird' plant. (**B**–**I**) Representative aneuploid lines showing variation in style/stigma and anther morphology. Scale bars: 1 cm in longitudinal flower section (**A**); 0.1 cm in style/stigma and anther close-ups (**B**–**I**).

Leaves of aneuploid lines were overall comparable in shape to those of the control, with no pronounced morphological or developmental abnormalities (Table 2 and Supplementary Fig. S1). Although leaf length and width were slightly larger in some individuals, these differences were inconsistent across lines. Similarly, stomatal traits displayed only modest variation, with occasional increases in stomatal length or guard cell width, whereas stomatal density was highly variable and lacked a consistent pattern. Together, these observations suggest that, in the lines examined here, leaf and epidermal traits were less consistently affected by chromosomal imbalance than floral traits.

For downstream analyses, severity groups were defined a priori using explicit reproductive and developmental criteria. Lines were classified as Severe if they failed to reach full anthesis and showed complete male sterility (pollen viability = 0% and germination = 0%). Lines that reached anthesis and retained non-zero viability and/or germination (viability > 0% and/or germination > 0%) were classified as Intermediate. The control 'Blue Bird' was designated as Normal. Notably, Pink-3 met the intermediate floral criteria but showed complete male sterility; therefore, it was treated as a borderline line and explicitly evaluated in sensitivity checks.

3.2 Cytogenetic Confirmation of Aneuploidy

Flow cytometry (FCM) of regenerated lines revealed fluorescence peaks that were consistently shifted to higher fluorescence intensity compared to the tetraploid 'Blue Bird' control, but did not correspond to exact whole-genome doubling (Table 2 and Fig. 3). Somatic chromosome counts from root tip spreads confirmed the aneuploid status of all eight surviving lines. Chromosome numbers deviated from the tetraploid complement (2n = 4x = 84 for 'Blue Bird') through gains or losses of multiple chromosomes, with pink lines exhibiting 154–182 chromosomes and white lines showing 150 chromosomes (Table 2). The relative genome size values of pink-flowered aneuploids (Pink 1–5) ranged from ~1.8× to 2.2× that of the control, while those of white-flowered aneuploids (White 1–3) were consistently ~1.8×.

Fluorescence *in situ* hybridization (FISH) was performed on one representative aneuploid line (pink-1, 2n = 154), using 45S and 5S rDNA probes (Fig. 3). In this representative line, the number of 45S and 5S signals appeared higher than in the tetraploid control, providing an illustrative example of rDNA signal patterns under aneuploidy. Because FISH was conducted on a single line, these signal patterns are not interpreted as a population-level feature of all aneuploid lines. Together, FCM and chromosome counting support the conclusion that all phenotypically divergent plants retained from antimitotic treatments were aneuploids rather than stable euploid polyploids.

3.3 Defects in Male Fertility in Aneuploids

Pollen size distributions revealed pronounced deviations in aneuploid lines compared with the control 'Blue Bird' (Table 3 and Fig. 4A). In the control, pollen diameters were narrowly distributed around 127.16 ± 9.88 μm, whereas pink-flowered aneuploids exhibited a broader distribution with a subset of abnormally large grains (>180 μm; operationally defined here as "giant pollen"). Pink-3, in particular, produced a small number of extremely large grains (194.51 ± 41.70 μm) alongside many misshapen forms. White-flowered aneuploids showed markedly reduced mean pollen size (86.50–111.59 μm) with high variance, consistent with structural abnormalities. The lower frequency of extremely large grains in white lines likely reflects that many grains did not develop sufficiently to be measured. In White 1–3 and Pink-3, pollen formation was strongly impaired such that total counts were reduced, and only grains with sufficiently intact walls to permit measurement were included in diameter statistics. Summary statistics are

reported for the measured pollen population; outlier handling followed the predefined rule described in Section 2.9.

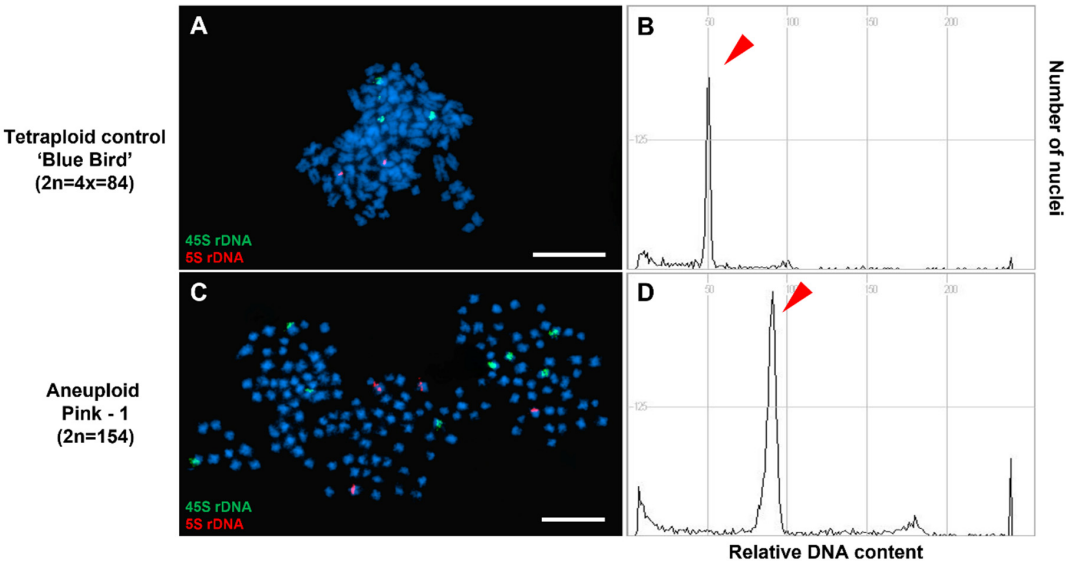

Figure 3: Cytogenetic characterization of a representative aneuploid line in *H. syriacus*. (**A**,**B**) Tetraploid control 'Blue Bird' (2n = 4x = 84) showing expected rDNA-FISH signals [45S (green), 5S (red)] and a stable DNA-content peak. (**C**,**D**) Representative aneuploid line Pink-1 (2n = 154) showing rDNA-FISH signal patterns and a shifted flow-cytometry profile relative to the control. Red arrowheads indicate the offset between nuclear DNA-content peaks between control and aneuploid plants, reflecting altered genome size. Scale bars = 10 µm.

Table 3: Pollen traits (viability, germination, and diameter; mean ± SD) in control and aneuploid *Hibiscus* lines. For viability and germination, at least 100 pollen grains were scored per replicate, and values represent means of three biological replicates (each based on multiple microscopic fields). Diameter was measured from ≥100 pollen grains per plant.

Sample	Viability (%)	Germination (%)	Diameter (µm)
'Blue Bird'	96.6 ± 2.6	8.9 ± 2.4	127.2 ± 9.9
Pink-1	73.7 ± 3.3	5.9 ± 2.1	139.6 ± 24.9
Pink-2	71.2 ± 3.4	2.5 ± 2.2	125.3 ± 20.3
Pink-3	0.0 ± 0.0	0.0 ± 0.0	194.5 ± 41.7
Pink-4	22.3 ± 9.9	0.0 ± 0.0	141.5 ± 38.6
Pink-5	14.3 ± 4.0	7.3 ± 1.8	152.7 ± 31.6
White-1	0.0 ± 0.0	0.0 ± 0.0	86.4 ± 9.0
White-2	0.0 ± 0.0	0.0 ± 0.0	86.5 ± 29.3
White-3	0.0 ± 0.0	0.0 ± 0.0	111.6 ± 13.4

Alexander staining confirmed significant viability loss in all aneuploid lines (Table 3 and Fig. 4B,C). Control pollen showed 96.60 ± 2.61% viability, whereas pink-flowered lines ranged from 73.69 ± 3.31% (Pink-1) to 14.26 ± 4.03% (Pink-5). All three white lines, as well as Pink-3, showed 0% viability. *In vitro* germination assays further indicated functional impairment (Fig. 4B,D). Control pollen readily germinated (8.91 ± 2.42%) and produced elongated tubes in which two sperm nuclei were visible upon DAPI staining, consistent with normal male gamete formation. In contrast, germination was sporadic and tubes were often

stunted or malformed in pink lines (2.52–7.25%) and was absent in all severe white lines and Pink-3. Together, these results indicate that, in the analysed aneuploid lines, chromosome dosage imbalance is associated with disruption across multiple stages of male gametophyte development, from microsporogenesis to pollen tube growth, with the strongest defects observed in lines showing the most pronounced floral abnormalities.

In the intermediate lines, viable pollen grains were detected by Alexander staining (Fig. 4B,C). In the micrographs, some viable grains appeared larger than surrounding inviable grains; however, pollen diameter measurements were performed on the overall pollen population and were not stratified by viability status. Because viability and germination were quantified independently of pollen-size outlier screening, the key fertility conclusions do not hinge on a small number of extreme-size grains.

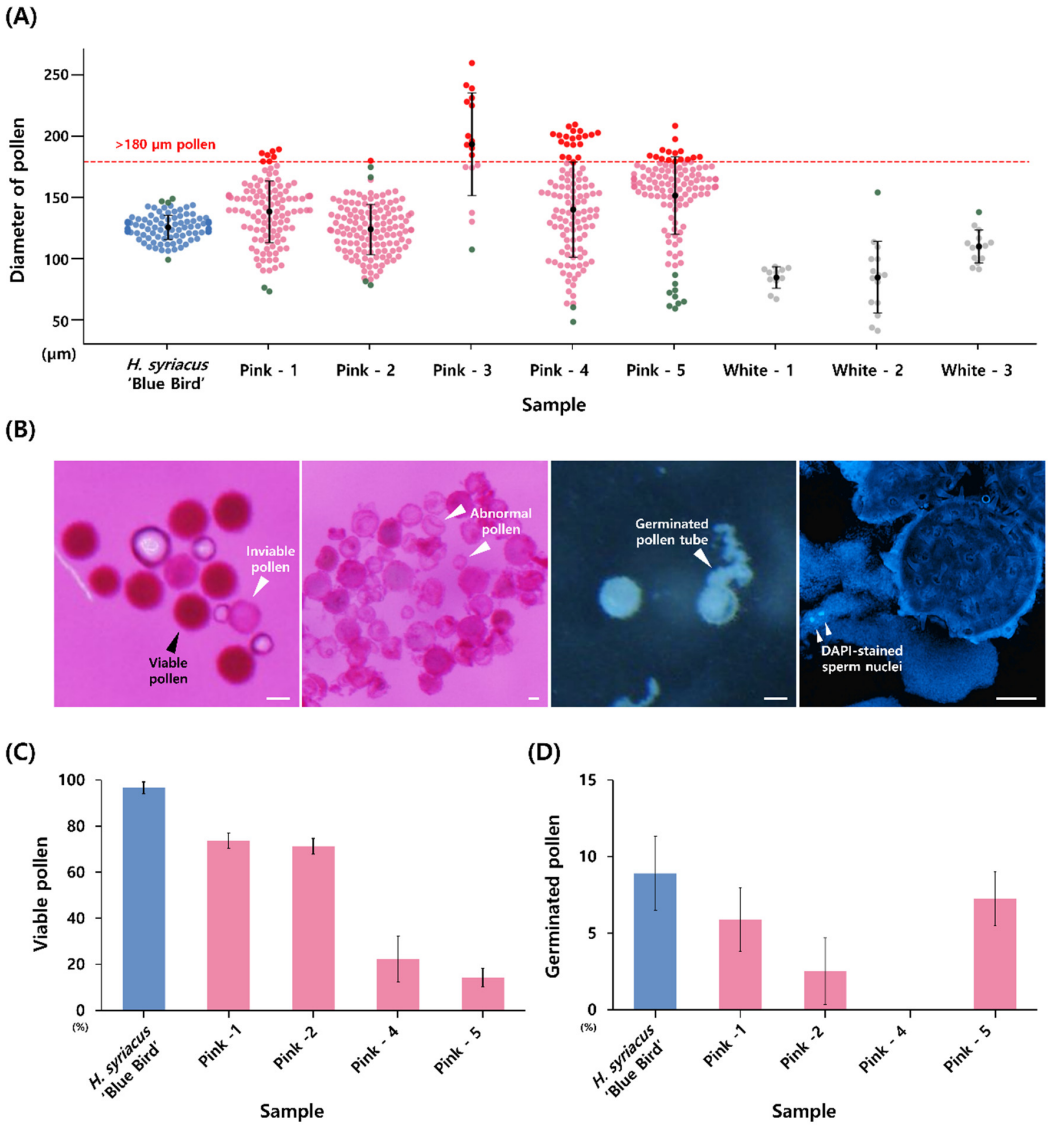

Figure 4: Pollen variation and male fertility. (**A**) Pollen diameter distributions across samples; dashed line marks large-pollen threshold. (**B**) Representative Alexander staining and *in vitro* germination images. (**C**) Viable pollen (%) and (**D**) germinated pollen (%). Bars indicate mean ± SD; n (grains per sample) reported in text. Scale bars: 100 μm in Alexander viability test and *in vitro* germinated close-ups; 50 μm in DAPI-stained sperm nuclei close-ups.

3.4 Meiotic and Post-Meiotic Abnormalities

Cytological examination of male gametogenesis showed that pachytene-stage chromosome configurations in aneuploid lines (Fig. 5A,B) were largely comparable to those of the control 'Blue Bird', with no conspicuous irregularities in pairing or synapsis. In contrast, abnormalities became pronounced at and after the tetrad stage. Aneuploid lines predominantly produced polyads with unevenly sized microspores (Fig. 5C,D and Supplementary Fig. S3). Post-meiotic stages in aneuploid lines (Fig. 5E,F) showed, in contrast to the uniform, regularly shaped pollen of the control, highly variable and irregular grain size and morphology.

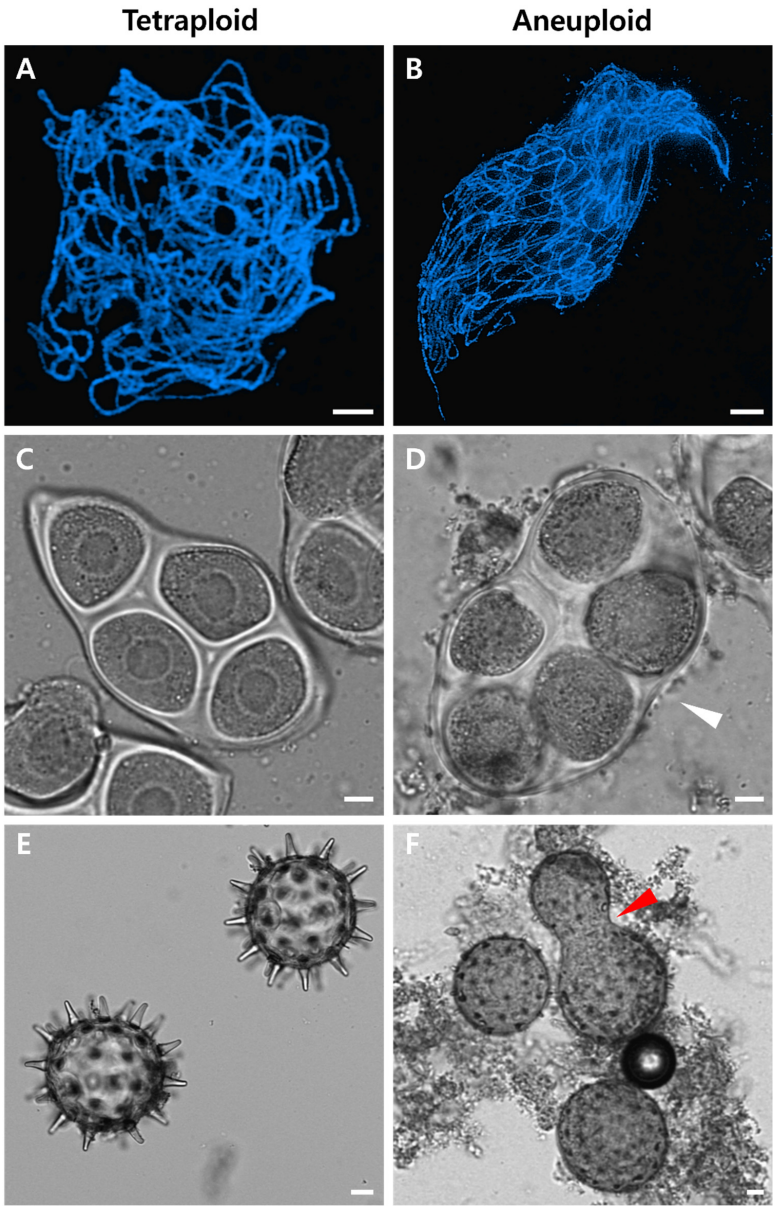

Figure 5: Cytological and pollen morphological abnormalities in aneuploid *H. syriacus*. (**A**,**B**) Pachytene spreads (no overt differences); (**C**,**D**) tetrads with irregular partitions in aneuploids (white arrow); Additional examples of polyads illustrating the wide morphological variability observed in aneuploids are presented in Supplementary Fig. S3. (**E**,**F**) malformed and heterogeneous pollen (red arrow). Scale bars = 10 μm.

These phenotypes (polyads/uneven microspores and irregular pollen morphology) were observed across the aneuploid lines examined, regardless of floral phenotype category. Because the incidence and severity varied widely even within a single anther, quantitative scoring was not feasible. Accordingly, Fig. 5 presents representative images at pachytene, tetrad, and mature pollen stages to illustrate the spectrum of meiotic and post-meiotic defects observed in association with chromosome imbalance in *H. syriacus*.

3.5 Petal Marker Gene Expression Across Severity Groups

Quantitative RT-PCR analysis revealed distinct expression patterns of the anthocyanin biosynthesis genes DFR and F3′5′H across phenotypic severity groups (Table 4 and Supplementary Table S2). In all aneuploid lines, DFR expression was strongly downregulated relative to the control 'Blue Bird' (fold change 0.00–0.09; $p < 0.001$), with no significant difference in suppression between intermediate (Pink 1–3) and severe (White 1–3) categories. In contrast, F3′5′H expression varied more widely, with Pink-2 showing moderate downregulation (fold change 0.05; $p < 0.05$), whereas other pink and white lines did not differ significantly from the control. Log10-transformed relative expression values ($2^{-\Delta\Delta Ct}$) confirmed these trends (Fig. 6), with Tukey's HSD grouping DFR expression of all aneuploids into a distinct, lower-expression subset apart from the control, while F3′5′H values showed partial overlap between groups.

Table 4: Quantitative qRT-PCR analysis of target gene expression. Data represent the relative expression levels (fold change) normalized to the expression of housekeeping gene (18S rRNA). ΔΔCt values and their corresponding standard deviation (SD) are shown. The fold change was calculated using the $2^{-\Delta\Delta Ct}$ method, with control samples serving as the baseline (fold change = 1).

Gene	Sample		Fold Change ($2^{-\Delta\Delta Ct}$)	Expression Trend	*p*-Value (ANOVA)
DFR	Tetraploid (control)	*H. syriacus* 'Blue Bird'	1.00		
	Aneuploid	Pink-1	0.02	Strongly downregulated	$p < 0.001$
		Pink-2	0.09	Strongly downregulated	$p < 0.001$
		Pink-3	0.05	Strongly downregulated	$p < 0.001$
		White-1	0.00	Strongly downregulated	$p < 0.001$
		White-2	0.02	Strongly downregulated	$p < 0.001$
		White-3	0.01	Strongly downregulated	$p < 0.001$
F3′5′H	Tetraploid (control)	*H. syriacus* 'Blue Bird'	1.00		
	Aneuploid	Pink-1	0.25	Not significant	$p > 0.05$
		Pink-2	0.05	Moderately downregulated	$p < 0.05$
		Pink-3	0.39	Not significant	$p > 0.05$
		White-1	0.38	Not significant	$p > 0.05$
		White-2	0.34	Not significant	$p > 0.05$
		White-3	0.54	Not significant	$p > 0.05$

Expression trends are categorized as "Strongly downregulated" or "Moderately downregulated" based on fold changes. ANOVA *p*-values are provided to indicate statistical significance ($p < 0.05$).

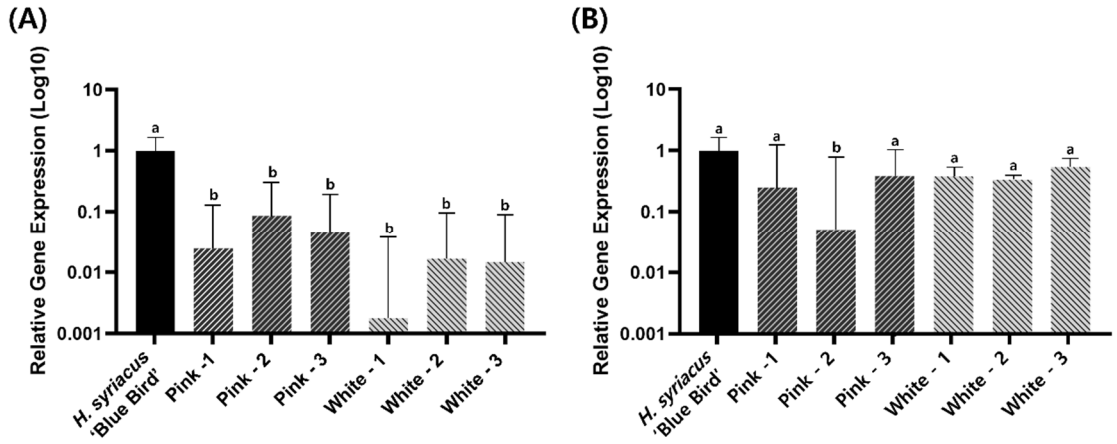

Figure 6: Relative gene expression analysis by RT-qPCR of (A) DFR and (B) F3′5′H in petal tissue. Relative expression levels ($2^{-\Delta\Delta Ct}$) are shown for the control, intermediate (pink), and severe (white) groups. Bars represent the mean ± SD of biological replicates, each with technical replicates. Different letters indicate significant differences according to Tukey's HSD.

3.6 Integrative Analysis of Morphology-Cytology-Fertility Relationships in Aneuploids

A radar plot summarizing min-max normalized mean values for eight floral and reproductive traits across the three severity groups (Normal, Intermediate, Severe) revealed distinct, severity-dependent phenotypic profiles (Fig. 7A). The severe group traced a markedly contracted polygon relative to the control for most traits, with minimal values for flower diameter, pollen germination, pollen viability, anther development, stigma development, and DFR gene expression, but showed the highest non-anther organ proportion (NAOP). Intermediate lines formed an intermediate-sized polygon, retaining partial performance in most traits but remaining below control levels. Notably, both intermediate and severe groups exhibited higher NAOP and larger mean pollen size compared with the control, despite severe reductions in fertility-related parameters. Both anthocyanin biosynthesis genes (DFR and F3′5′H) showed reduced expression in aneuploid groups, with DFR suppression particularly pronounced and uniform across intermediate and severe categories.

To further integrate trait variation at the individual-plant level, PCA was performed using nine floral and reproductive traits. The first two PCs explained 82.6% of the variance (PC1 = 65.2%, PC2 = 17.4%). Along PC1, the control (*H. syriacus* 'Blue Bird') separated strongly from all aneuploids, reflecting its higher fertility and floral trait values. Severe aneuploids clustered together with negative PC1 scores, distinguished by reduced fertility traits and higher NAOP, whereas intermediate lines occupied intermediate positions between normal and severe classes. Trait loading vectors indicated that DFR expression, pollen viability, and pollen germination contributed most positively to PC1, while NAOP loaded strongly in the opposite direction (Fig. 7B). These results indicate coordinated co-variation among cytological, morphological, and molecular traits within the analysed aneuploid lines, and are consistent with a severity-dependent pattern.

As a sensitivity check, PCA was repeated after excluding Pink-3; the overall structure of the ordination (control vs. aneuploids and intermediate vs. severe separation) was retained, while the variance explained by the first two components increased from 82.6% (PC1 65.2%, PC2 17.4%; n = 7) to 91.8% (PC1 73.7%, PC2 18.1%; n = 6).

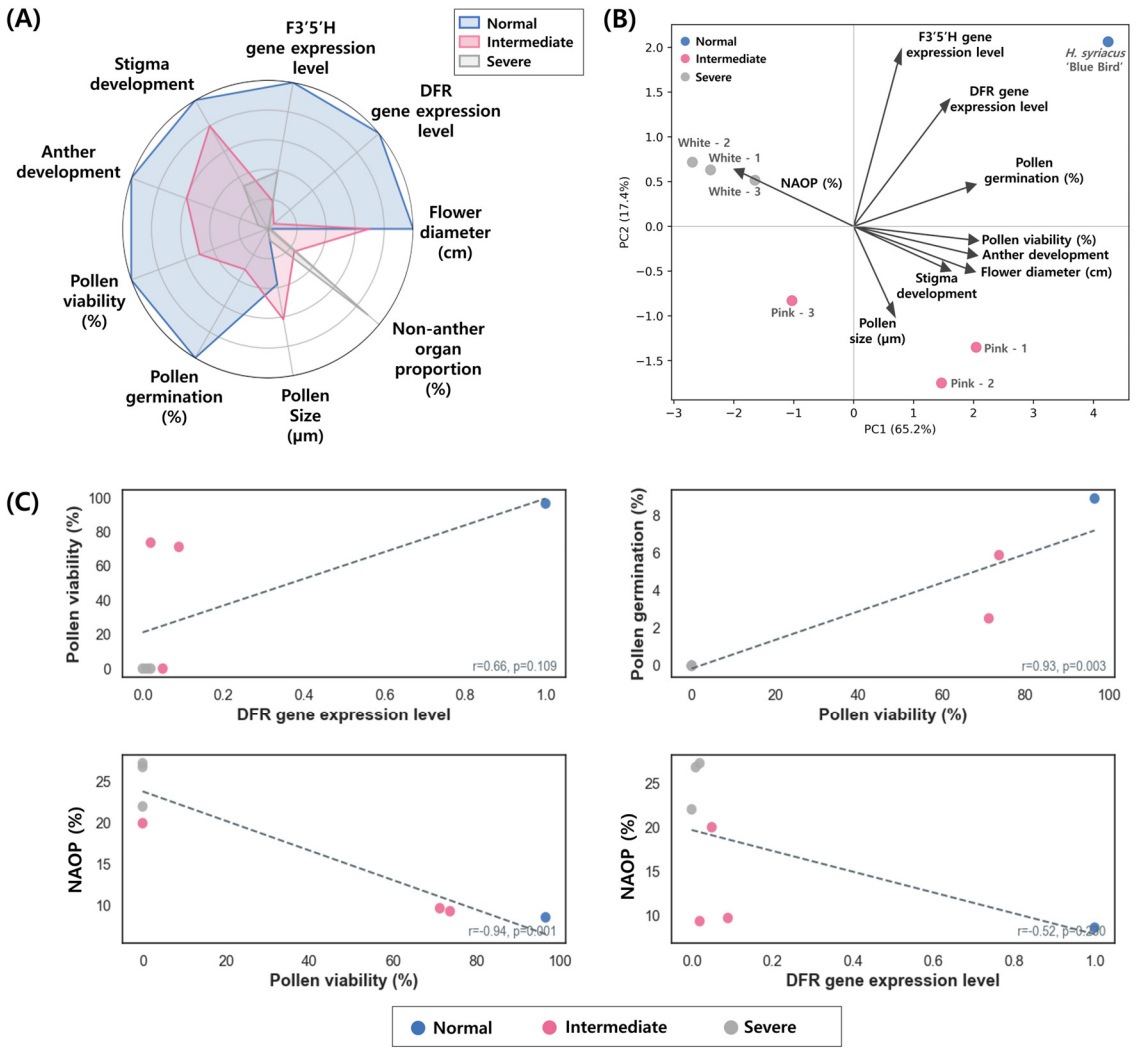

Figure 7: Integrative multi-trait analyses linking cytology, morphology, and fertility in control and aneuploid *H. syriacus*. (**A**) Radar plot summarizing group-level divergence (Normal, Intermediate, Severe) across nine phenotypic and molecular traits. (**B**) Principal component analysis (PCA) biplot integrating all traits, showing separation of control and aneuploid individuals along PC1 (65.2%) and PC2 (17.4%). Trait loadings are indicated by arrows. (**C**) Pairwise correlation plots among representative variables (e.g., DFR expression vs. pollen viability; pollen viability vs. germination; NAOP vs. pollen viability/DFR). Dashed lines show least-squares fits; Pearson's r and *p* values are indicated. NAOP (%) = Non-anther organ proportion.

Correlation analysis among phenotypic and molecular traits identified four representative relationships with the strongest effect sizes or statistical support (Fig. 7C). Pollen germination rate was positively correlated with pollen viability (r = 0.93, $p = 0.003$), while NAOP showed a strong negative correlation with pollen viability (r = −0.94, $p < 0.01$). DFR gene expression exhibited a positive, though not statistically significant association with pollen viability (r = 0.66, $p = 0.109$), and a weaker negative correlation with NAOP (r = −0.52, $p = 0.20$). These patterns are consistent with co-variation of floral organ composition (including reduced anther development), male gametophyte function, and anthocyanin pathway gene expression across severity classes, with the most severe lines combining high NAOP with low viability and germination.

4 Discussion

4.1 Chromosome Dosage Imbalance Is Associated with Multifaceted Phenotypic Changes

Aneuploidy, defined as the presence of an abnormal number of chromosomes, is widely associated with altered expression balance across many genes [9,27]. Such dosage imbalance has been linked to diverse effects on morphology, physiology, and development in a range of plant systems. In the *Hibiscus* aneuploid lines analysed here, these differences were most evident in reproductive traits, including flower size, pigmentation, and floral organ composition, whereas vegetative traits such as leaf morphology showed only subtle and inconsistent variation (Figs. 1 and 2).

These phenotypic differences are commonly discussed in relation to gene dosage effects, altered transcript abundance of genes located on dosage-varied chromosomes, and downstream responses of dosage-sensitive regulatory networks [28,29]. However, these mechanisms were not directly tested in the present study. Accordingly, the patterns observed here are more appropriately interpreted as being consistent with chromosome dosage imbalance rather than as direct evidence of a specific mechanistic pathway.

Dosage-associated phenotypic changes have been documented in other plant species. In wheat, the addition or loss of specific chromosomes or chromosome arms has been associated with reduced plant height, altered spike morphology, delayed heading, and decreased seed set [30]. In maize, B-chromosome and A-chromosome dosage series have likewise shown that monosomic or trisomic states can be accompanied by changes in leaf size, chlorophyll content, flowering time, and tassel architecture [29]. Similarly, in *Arabidopsis*, segmental aneuploid lines have shown reduced organ size, delayed floral transition, and fertility defects, together with broad transcriptional imbalance [8]. The *Hibiscus* aneuploid lines analysed here are consistent with these general patterns at the floral and reproductive levels, particularly in showing reduced flower size, shifts in floral organ composition, occasional petaloid structures, and marked reductions in male fertility. Within the present dataset, these results support the interpretation that chromosome dosage imbalance was accompanied by coordinated disruption of floral and reproductive traits.

4.2 DFR Downregulation Is Consistent with Altered Flower Pigmentation

The strong and uniform downregulation of DFR observed across all aneuploid lines suggests that this gene is highly dosage-sensitive within the anthocyanin biosynthesis pathway (Fig. 6). Given that only two targets were assayed, these qRT-PCR results should be interpreted as a targeted signal consistent with reduced anthocyanin biosynthetic capacity, rather than as definitive evidence of the sole causal mechanism underlying the color shift. The lack of a significant change in F3′5′H suggests that the observed expression pattern is compatible with a bottleneck at the DFR step, although upstream regulators and additional pathway genes were not evaluated here.

Dihydroflavonol 4-reductase (DFR) catalyzes a key step by reducing dihydroflavonols to leucoanthocyanidins, which are direct precursors of colored anthocyanins [31]. This enzyme plays a crucial role in determining pigment intensity and flower coloration in many species, including *Arabidopsis*, rose, and *Petunia* [32–34]. Thus, the consistent reduction of DFR transcript levels in aneuploids is consistent with a generalized decrease in anthocyanin biosynthetic capacity and may contribute to the pale or altered flower colors observed in the *Hibiscus* aneuploid lines (Fig. 6). However, because only two pathway genes were assayed and pigment levels were not quantified, this interpretation remains provisional and does not exclude involvement of upstream regulators or additional biosynthetic steps.

In contrast, F3′5′H (flavonoid 3′,5′-hydroxylase) showed variable expression patterns among aneuploid lines (Figs. 1, 2 and 6). This gene encodes a cytochrome P450 enzyme that hydroxylates dihydroflavonols

to produce delphinidin-based anthocyanins responsible for blue and violet hues [35]. The differential downregulation observed, particularly the moderate reduction in only one intermediate line (Pink-2), is consistent with heterogeneity among aneuploid lines and may reflect line-specific dosage and/or regulatory differences affecting F3′5′H expression. However, locus-level copy-number or structural differences were not evaluated in this study [36].

Notably, several studies in ornamental crops have reported that prolonged exposure to high temperatures can suppress anthocyanin accumulation and result in paler floral pigmentation [37,38]. This raises the possibility that unmeasured seasonal or cultivation variation could have influenced absolute colour intensity in our control plants at the time of sampling. In our local cultivation conditions during the 2025 season, the control 'Blue Bird' flowers appeared visually paler than expected for this cultivar; however, because temperature exposure and pigment intensity were not quantified and no multi-season replication was performed, this observation remains anecdotal and cannot be used to explain gene-expression patterns. Accordingly, the qRT-PCR results are interpreted primarily as a targeted signal from a restricted gene set rather than as a definitive mechanism for colour determination.

Dose-sensitive regulation of key biosynthetic genes such as DFR reflects their pivotal roles as pathway bottlenecks, whereas peripheral enzymatic genes may better tolerate dosage variation due to compensatory mechanisms like epigenetic regulation or gene redundancy [39]. Similar dosage sensitivity patterns in anthocyanin biosynthesis genes have been reported previously [40], consistent with the possibility that chromosomal imbalance may affect pigment-related pathways and may contribute to a spectrum of floral color phenotypes. In addition, the co-occurrence of heat stress and chromosomal imbalance in our growing conditions raises a testable hypothesis that abiotic stress could interact with dosage imbalance to modulate pigment stability; this will require targeted experiments (e.g., controlled-temperature trials and pigment quantification) in future work.

4.3 Meiotic Irregularities and Reduced Male Fertility in Aneuploids

Aneuploidy in *H. syriacus* was associated with disruption of male reproductive development, as reflected by meiotic irregularities and compromised pollen formation in the analysed lines. Although pachytene-stage cells did not show readily discernible differences from the control, abnormalities became apparent during and after meiotic divisions, with polyads and uneven microspores frequently observed (Fig. 5 and Supplementary Fig. S3). These phenotypes are consistent with irregular chromosome segregation during meiosis and could contribute to malformed, inviable pollen grains that display diverse size abnormalities, ranging from abnormally large to shrunken or aborted forms (Fig. 5) [41,42].

The strong reduction in pollen viability and germination rates across the aneuploid lines was consistent with the presence of meiotic and post-meiotic abnormalities observed in this study (Figs. 4 and 5). More broadly, aneuploidy entails imbalanced gene dosage, which has been associated in other plant systems with altered regulation of chromosome segregation and gamete maturation [43,44]. Disrupted expression of genes controlling microtubule dynamics, spindle assembly, and meiotic checkpoints may contribute to the observed abnormalities [45–47], although these molecular pathways were not directly examined here and remain to be characterized in *H. syriacus* aneuploids.

Similar meiotic instability and fertility reduction have been documented in other crops. For instance, wheat monosomics frequently exhibit lagging chromosomes and micronuclei during pollen meiosis [48], and in maize, segmental aneuploidy affecting portions of chromosome 5 and 6 has been associated with abnormal tassel architecture and reduced fertility [49]. In *Arabidopsis*, chromosome gains or losses can impair pollen viability and seed set [8].

Taken together, these observations suggest that meiotic instability may be one contributing factor to reduced male fertility in the *Hibiscus* aneuploid lines analysed here. However, given the limited number of evaluable lines and the observational nature of the cytological scoring, these results should be interpreted as associations within this dataset rather than as definitive evidence for a single causal pathway. The findings nonetheless emphasize that chromosome dosage imbalance can pose constraints on successful male gametogenesis, which is relevant when considering the breeding and horticultural use of aneuploid plants.

4.4 Floral Organ Identity Shifts and Homeotic-Like Features

The increased NAOP observed in the severe aneuploid *H. syriacus* lines (Figs. 2 and 7; Supplementary Fig. S2) was consistent with marked changes in floral organ composition, including reduced anther development and the occurrence of petal-like structures within the stamen whorl. In this study, NAOP was defined as the proportion of floral organs that are not anthers relative to the total number of counted floral organs, thereby capturing the relative reduction of androecium contribution within the overall floral organ set rather than absolute petal number. As used here, this metric provides a simple quantitative summary of reduced anther representation relative to the total floral organ set and may serve as an operational indicator of androecium disruption among the analysed lines.

These patterns are consistent with altered floral organ identity or developmental regulation [27,50], although the underlying molecular basis was not directly examined in this study. More broadly, dosage-sensitive regulatory imbalance is a well-recognized consequence of genomic imbalance [51]. Floral organ identity is commonly discussed in relation to the MADS-box family of transcription factors, which act in combinatorial complexes within the classical ABC/ABCDE framework to specify sepals, petals, stamens, and carpels [52–55]. In other systems, altered dosage or expression of these regulatory genes has been associated with homeotic transformations [56]. The organ-identity alterations observed here, including petal-like organs within the stamen whorl and altered petal morphology, are therefore compatible with a homeotic-like interpretation, but this should be regarded as a proposed explanation rather than as a demonstrated mechanism.

MADS-box gene expression was not examined in the present work, in part because flowering in the severe aneuploid lines was limited and the primary focus of the study was on fertility-related phenotypic and cytological traits. Accordingly, a detailed molecular or quantitative analysis of stamen petaloidy and related floral identity phenotypes was beyond the scope of this study. Future work could test this interpretation more directly through targeted expression profiling of floral identity regulators in flowering aneuploid lines under controlled conditions. Such analyses would help determine whether the observed floral phenotypes reflect altered organ identity programs, broader developmental imbalance, or a combination of both.

4.5 Integrative Multivariate Analysis of Phenotypic and Molecular Traits

Given the limited number of evaluable flowering lines, the multivariate analyses in this study were used in an exploratory manner to summarize covariation among the measured phenotypic and molecular traits in aneuploid lines of *H. syriacus* (Fig. 7B). The PCA revealed that the first two principal components together explained 82.6% of the total variance (PC1 = 65.2%, PC2 = 17.4%). Along PC1, the control cultivar (‘Blue Bird’) was separated from the aneuploid groups, consistent with differences in fertility-related, floral, and pigmentation-associated variables included in the analysis [49]. The intermediate and severe lines were positioned in the negative PC1 space, where lower pollen viability, lower germination, and reduced floral organ development tended to co-occur with higher NAOP values and altered pollen size.

Correlation analyses further provided a descriptive summary of pairwise relationships among the measured traits (Fig. 7C). Pollen viability and germination showed a strong positive association, whereas NAOP showed a strong negative association with pollen viability. A positive but weaker association was also observed between DFR expression and fertility-related parameters. However, these relationships should be interpreted as exploratory co-variation within the analysed lines rather than as evidence of directional or mechanistic links [29]. Radar plots likewise provided a visual summary of severity-dependent trait differences, with the severe group showing contraction across most measured axes relative to the control (Fig. 7A) [57].

A sensitivity analysis excluding Pink-3, which represented a borderline case in terms of floral phenotype and male sterility, retained the overall ordination structure while increasing the proportion of variance explained by the first two components. This result indicates that the observed PCA pattern in the present dataset was not driven solely by that line. Nevertheless, because the number of analysed lines remained small, this sensitivity check should be regarded as an internal robustness assessment within the dataset rather than as evidence of broader generality.

Taken together, these multivariate analyses suggest coordinated variation among floral morphology, organ composition, fertility-related traits, and targeted gene-expression signals within the analysed lines. However, they do not establish causal or unifying mechanisms. Instead, they provide an exploratory framework that complements the cytological and gene-expression observations and may help guide future studies using larger populations and broader molecular characterization.

4.6 Implications for Hibiscus Breeding and Ornamental Horticulture

The characterization of aneuploid individuals recovered during artificial polyploidy induction in *H. syriacus* provides practical guidance for breeding pipelines, even if these lines have limited immediate commercial value. The combination of reduced fertility, meiotic instability, and altered floral morphology observed here illustrates common risks associated with chromosomal imbalance during chromosome manipulation. Similar outcomes have been reported in induced polyploidy efforts in other systems, underscoring the need for early cytogenetic triage when advancing candidate lines [58,59].

From a breeding perspective, the present phenotypic and cytological documentation provides an empirical basis to develop practical criteria for distinguishing chromosomal constitutions that are more tolerable from those that are accompanied by severe reproductive dysfunction. Such screening is particularly relevant in early generations of chromosome manipulation, when unbalanced karyotypes and mixoploids can be frequent. Flow cytometry offers a rapid and cost-effective first-pass screen to flag genome-size shifts, detect aneuploid or mixoploid cytotypes, and prioritize material for chromosome counting and subsequent evaluation [60,61]. In this context, the treatment-level recovery outcomes summarized in Table 1 can serve as a useful starting point for designing induction and screening pipelines.

Importantly, while many aneuploid lines are expected to show reduced reproductive fitness, aneuploidy can occasionally generate visually distinctive floral phenotypes (e.g., altered pigmentation intensity or patterning, altered organ morphology) that may be of horticultural interest. In *H. syriacus*, however, such variants would still require rigorous selection for vegetative performance and flowering stability before breeding value can be claimed. Accordingly, within chromosome-engineering pipelines, induced aneuploidy is more realistically positioned as a source of phenotypic variation and a tool for identifying dosage-sensitive developmental processes, rather than as a direct route to cultivar release.

These findings also inform fertility-recovery strategies. When aneuploidy depresses male function, breeders can consider backcrossing to euploid parents and selecting progeny with more balanced

chromosome complements, guided by routine flow-cytometric screening [62–65]. Such approaches can, in principle, help recover fertility while maintaining useful phenotypic variation introduced during chromosome manipulation.

Given that only a subset of regenerated lines reached flowering maturity, our conclusions should be interpreted primarily as associations within the analysed lines, and broader generalization will require validation in larger populations. In sum, the value of these aneuploid materials is primarily methodological rather than immediate: they refine screening criteria, clarify failure modes that erode fertility, and provide dosage-perturbation models that may support future trait-chromosome association efforts as genomic and cytogenetic resources improve [66,67].

5 Conclusion

In this study, a subset of regenerated *Hibiscus syriacus* 'Blue Bird' lines showing genome-size shifts after antimitotic treatment reached flowering maturity and was characterized in detail. Across these analysed aneuploid lines, floral alterations and male fertility impairment co-occurred with cytological abnormalities during late microsporogenesis and post-meiotic development. Functional assays (pollen viability and germination) consistently indicated substantial reductions in male fertility relative to the control, while targeted qRT-PCR of two anthocyanin-pathway genes provided a limited signal aligned with the observed pigmentation changes, particularly the uniform downregulation of DFR. A representative rDNA-FISH profile is presented as an illustrative cytogenetic example for one line and does not imply generalizable rDNA copy changes across all aneuploids. Overall, these results support the view that induced aneuploidy in *H. syriacus* is accompanied by coordinated reproductive and floral phenotypes within the material examined here, and they underscore the practical value of early flow-cytometric screening combined with targeted cytology to inform selection and reduce the likelihood of advancing unstable karyotypes in ornamental breeding pipelines.

Acknowledgement: Not applicable.

Funding Statement: This work was supported by Korea Institute of Planning and Evaluation for Technology in Food, Agriculture and Forestry (IPET) through Technology Commercialization Support Program, funded by Ministry of Agriculture, Food and Rural Affairs (MAFRA) (RS-2024-00399700).

Author Contributions: Yun-Jae Ahn conceptualized the study, curated the data, conducted the investigation, supervised the work, and wrote the original draft and subsequent revisions. Moon-Seok Kang conducted data acquisition, formal analysis, and investigation. Ki-Byung Lim acquired funding, provided resources, and supervised the study. All authors reviewed and approved the final version of the manuscript.

Availability of Data and Materials: The authors confirm that the data supporting the findings of this study are available within the article and its Supplementary Materials.

Ethics Approval: Not applicable.

Conflicts of Interest: The authors declare no conflicts of interest.

Supplementary Materials: The supplementary material is available online at https://www.techscience.com/doi/10.32604/phyton.2026.078884/s1.

Abbreviations

ANOVA	analysis of variance
DAPI	4′,6-diamidino-2-phenylindole
DFR	dihydroflavonol 4-reductase
F3′5′H	flavonoid 3′,5′-hydroxylase
FCM	flow cytometry
FISH	fluorescence *in situ* hybridization
HSD	honestly significant difference (Tukey's HSD)
PCA	principal component analysis
NAOP	Non-anther organ proportion
qRT-PCR	quantitative real-time polymerase chain reaction
RHS	Royal Horticultural Society colour chart
SD	standard deviation

References

1. Yali W. Polyploidy and its importance in modern plant breeding improvement. Int J Agric Biosci. 2022;11(1):53–8. [CrossRef].
2. Fu L, Zhu Y, Li M, Wang C, Sun H. Autopolyploid induction via somatic embryogenesis in *Lilium distichum* Nakai and *Lilium cernuum* Komar. Plant Cell Tissue Organ Cult PCTOC. 2019;139(2):237–48. [CrossRef].
3. Ghanbari MA, Jowkar A, Salehi H, Zarei M. Effects of polyploidization on petal characteristics and optical properties of *Impatiens walleriana* (Hook.). Plant Cell Tissue Organ Cult PCTOC. 2019;138(2):299–310. [CrossRef].
4. Kushwah KS, Verma RC, Patel S, Jain NK. Colchicine induced polyploidy in *Chrysanthemum carinatum* L. J Phylogenet Evol Biol. 2018;6(1):193. [CrossRef].
5. Podwyszyńska M, Trzewik A, Marasek-Ciolakowska A. *In vitro* polyploidisation of tulips (*Tulipa gesneriana* L.)—Phenotype assessment of tetraploids. Sci Hortic. 2018;242:155–63. [CrossRef].
6. Taylor NL, Anderson MK, Quesenberry KH, Watson L. Doubling the chromosome number of *Trifolium* Species using nitrous Oxide[1]. Crop Sci. 1976;16(4):516–8. [CrossRef].
7. Wu Y, Sun Y, Sun S, Li G, Wang J, Wang B, et al. Aneuploidization under segmental allotetraploidy in rice and its phenotypic manifestation. Theor Appl Genet. 2018;131(6):1273–85. [CrossRef].
8. Henry IM, Dilkes BP, Miller ES, Burkart-Waco D, Comai L. Phenotypic consequences of aneuploidy in *Arabidopsis thaliana*. Genetics. 2010;186(4):1231–45. [CrossRef].
9. Makarevitch I, Harris C. Aneuploidy causes tissue-specific qualitative changes in global gene expression patterns in maize. Plant Physiol. 2010;152(2):927–38. [CrossRef].
10. Oleszczuk S, Rabiza-Swider J, Zimny J, Lukaszewski AJ. Aneuploidy among androgenic progeny of hexaploid *Triticale* (XTriticosecale Wittmack). Plant Cell Rep. 2011;30(4):575–86. [CrossRef].
11. Sevilleno SS, Cabahug-Braza RAM, An HR, Hwang YJ. Analyzing pollen fertility based on micronuclei presence in yellow aneuploid *Phalaenopsis*. Korean J Breed Sci. 2023;55(4):287–95. [CrossRef].
12. Go S, Koo H, Jung M, Hong S, Yi G, Kim YM. Pan-chloroplast genomes for accession-specific marker development in *Hibiscus syriacus*. Sci Data. 2024;11:246. [CrossRef].
13. Ha YM, Lim KB, Shim KK. Development of a new *Hibiscus cultivar* 'daewangchun' with vigorous growth and unique red eye through interspecific hybridization. Hortic Sci Technol. 2015;33(3):453–8. [CrossRef].
14. Kim YM, Kim S, Koo N, Shin AY, Yeom SI, Seo E, et al. Genome analysis of *Hibiscus syriacus* provides insights of polyploidization and indeterminate flowering in woody plants. DNA Res. 2017;24:71–80. [CrossRef].
15. Kuligowska K, Lütken H, Müller R. Towards development of new ornamental plants: Status and progress in wide hybridization. Planta. 2016;244(1):1–17. [CrossRef].
16. Wang X, Chen J, Hu L, Zhang J, Xiao F, Zhang S, et al. Embryological observations on seed abortion in *Hibiscus syriacus* L. and physiological studies on nutrients, enzyme activity and endogenous hormones. BMC Plant Biol. 2023;23(1):665. [CrossRef].
17. Li Z, Liu D, Wang D, Sun M, Zhang G, Wu Y, et al. Study on the causes of changes in colour during *Hibiscus syriacus* flowering based on transcriptome and metabolome analyses. BMC Plant Biol. 2024;24(1):431. [CrossRef].

18. Wang X, Li L, Liu C, Zhang M, Wen Y. An integrated metabolome and transcriptome analysis of the *Hibiscus syriacus* L. petals reveal the molecular mechanisms of anthocyanin accumulation. Front Genet. 2022;13:995748. [CrossRef].
19. Zhang J, Cheng C, Xiao F, Zhang X, Zhang C, Zhao Y, et al. Effects of ploidy level on leaf morphology, stomata, and anatomical structure of *Hibiscus syriacus* L. BMC Plant Biol. 2024;24(1):1133. [CrossRef].
20. Xu J, Shin JY, Park PM, An HR, Kim YJ, Kim SJ, et al. Flower color modification through co-overexpression of the VtF3′5′H and RhNHX genes in *Rosa* hybrida. Plant Cell Tissue Organ Cult PCTOC. 2023;153(2):403–16. [CrossRef].
21. Kirov I, Divashuk M, Van Laere K, Soloviev A, Khrustaleva L. An easy "SteamDrop" method for high quality plant chromosome preparation. Mol Cytogenet. 2014;7(1):21. [CrossRef].
22. Lim KB, Ramanna MS, de Jong JH, Jacobsen E, van Tuyl JM. Indeterminate meiotic restitution (IMR): A novel type of meiotic nuclear restitution mechanism detected in interspecific lily hybrids by GISH. Theor Appl Genet. 2001;103(2):219–30. [CrossRef].
23. Lawrence S, Pang Q, Kong W, Chen S. Stomata tape-peel: An improved method for guard cell sample preparation. J Vis Exp. 2018;(137):57422. [CrossRef].
24. Alexander MP. Differential staining of aborted and nonaborted pollen. Stain Technol. 1969;44(3):117–22. [CrossRef].
25. Burke JJ, Velten J, Oliver MJ. *In vitro* analysis of cotton pollen germination. Agron J. 2004;96(2):359–68. [CrossRef].
26. Wang C, Hou X, Qi N, Li C, Luo Y, Hu D, et al. An optimized method to obtain high-quality RNA from different tissues in *Lilium davidii* var. unicolor. Sci Rep. 2022;12:2825. [CrossRef].
27. Hou J, Shi X, Chen C, Islam MS, Johnson AF, Kanno T, et al. Global impacts of chromosomal imbalance on gene expression in *Arabidopsis* and other taxa. Proc Natl Acad Sci U S A. 2018;115(48):E11321–30. [CrossRef].
28. Huettel B, Kreil DP, Matzke M, Matzke AJM. Effects of aneuploidy on genome structure, expression, and interphase organization in *Arabidopsis thaliana*. PLoS Genet. 2008;4(10):e1000226. [CrossRef].
29. Shi X, Yang H, Chen C, Hou J, Hanson KM, Albert PS, et al. Genomic imbalance determines positive and negative modulation of gene expression in diploid maize. Plant Cell. 2021;33(4):917–39. [CrossRef].
30. Förster S, Schumann E, Baumann M, Weber WE, Pillen K. Copy number variation of chromosome 5A and its association with Q gene expression, morphological aberrations, and agronomic performance of winter wheat cultivars. Theor Appl Genet. 2013;126(12):3049–63. [CrossRef].
31. Han M, Yang C, Zhou J, Zhu J, Meng J, Shen T, et al. Analysis of flavonoids and anthocyanin biosynthesis-related genes expression reveals the mechanism of petal color fading of *Malus hupehensis* (Rosaceae). Braz J Bot. 2020;43(1):81–9. [CrossRef].
32. Cheng Y, Tian Y, Guo P, Luo J, Xu C, Zhang Y, et al. Novel insights into pigment composition and molecular mechanisms governing flower coloration in rose cultivars exhibiting diverse petal hues. Plants. 2024;13(23):3353. [CrossRef].
33. Chu YX, Chen HR, Wu AZ, Cai R, Pan JS. Expression analysis of dihydroflavonol 4-reductase genes in *Petunia hybrida*. Genet Mol Res. 2015;14(2):5010–21. [CrossRef].
34. Shin DH, Choi MG, Kang CS, Park CS, Choi SB, Park YI. Overexpressing the wheat dihydroflavonol 4-reductase gene TaDFR increases anthocyanin accumulation in an *Arabidopsis* dfr mutant. Genes Genom. 2016;38(4):333–40. [CrossRef].
35. Tanaka Y, Brugliera F. Flower colour and cytochromes P450. Phil Trans R Soc B. 2013;368(1612):20120432. [CrossRef].
36. Kojima S, Cimini D. Aneuploidy and gene expression: Is there dosage compensation? Epigenomics. 2019;11(16):1827–37. [CrossRef].
37. Alcantud R, Weiss J, Terry MI, Bernabé N, Verdú-Navarro F, Fernández-Breis JT, et al. Flower transcriptional response to long term hot and cold environments in *Antirrhinum majus*. Front Plant Sci. 2023;14:1120183. [CrossRef].
38. Wang F, Li Z, Wu Q, Guo Y, Wang J, Luo H, et al. Floral response to heat: A study of color and biochemical adaptations in purple chrysanthemums. Plants. 2024;13(13):1865. [CrossRef].
39. Shi J, Dong A, Shen WH. Epigenetic regulation of rice flowering and reproduction. Front Plant Sci. 2015;5:803. [CrossRef].

40. Chen ZJ. Genetic and epigenetic mechanisms for gene expression and phenotypic variation in plant polyploids. Annu Rev Plant Biol. 2007;58:377–406. [CrossRef].
41. Shin H, Park HR, Park JE, Yu SH, Yi G, Kim JH, et al. Reduced fertility caused by meiotic defects and micronuclei formation during microsporogenesis in xBrassicoraphanus. Genes Genom. 2021;43(3):251–8. [CrossRef].
42. Xiao K, Zhu Z, Zou N, Zhang L, Sun Y, Zhou S. The characteristics of abnormal meiosis and functional aneuploid pollen of odd-allotetraploid lily 'Honesty' unveiled using *in situ* hybridization. Sci Hortic. 2022;300:111091. [CrossRef].
43. Alexander L. Ploidy level influences pollen tube growth and seed viability in interploidy crosses of *Hydrangea macrophylla*. Front Plant Sci. 2020;11:100. [CrossRef].
44. Henry IM, Dilkes BP, Tyagi AP, Lin HY, Comai L. Dosage and parent-of-origin effects shaping aneuploid swarms in *A. thaliana*. Heredity. 2009;103(6):458–68. [CrossRef].
45. Bayley PM, Sharma KK, Martin SR. Microtubule dynamics *in vitro*. Microtubules. 1994;13:111–37.
46. Liu B, Lee YJ. Spindle assembly and mitosis in plants. Annu Rev Plant Biol. 2022;73:227–54. [CrossRef].
47. Zamariola L, Tiang CL, De Storme N, Pawlowski W, Geelen D. Chromosome segregation in plant meiosis. Front Plant Sci. 2014;5:279. [CrossRef].
48. Morrison JW, Unrau J. Frequency of micronuclei in pollen quartets of common wheat monosomics. Can J Bot. 1952;30(4):371–8. [CrossRef].
49. Makarevitch I, Phillips RL, Springer NM. Profiling expression changes caused by a segmental aneuploid in maize. BMC Genom. 2008;9(1):7. [CrossRef].
50. Krizek BA, Fletcher JC. Molecular mechanisms of flower development: An armchair guide. Nat Rev Genet. 2005;6(9):688–98. [CrossRef].
51. Birchler JA, Veitia RA. Gene balance hypothesis: Connecting issues of dosage sensitivity across biological disciplines. Proc Natl Acad Sci U S A. 2012;109(37):14746–53. [CrossRef].
52. Benedito VA, Angenent GC, van Tuyl JM, Krens FA. *Lilium longiflorum* and molecular floral development: The abcde model. Acta Hortic. 2004;651(651):83–9. [CrossRef].
53. Eckardt NA. MADS monsters: Controlling floral organ identity. Plant Cell. 2003;15(4):803–5. [CrossRef].
54. Theißen G. Development of floral organ identity: Stories from the MADS house. Curr Opin Plant Biol. 2001;4(1):75–85. [CrossRef].
55. Theißen G, Melzer R, Rümpler F. MADS-domain transcription factors and the floral quartet model of flower development: Linking plant development and evolution. Development. 2016;143(18):3259–71. [CrossRef].
56. Chen M, Nie G, Yang L, Zhang Y, Cai Y. Homeotic transformation from stamen to petal in *Lilium* is associated with *MADS*-box genes and hormone signal transduction. Plant Growth Regul. 2021;95(1):49–64. [CrossRef].
57. Cornea-Cipcigan M, Bunea A, Bouari CM, Pamfil D, Páll E, Urcan AC, et al. Anthocyanins and carotenoids characterization in flowers and leaves of *Cyclamen* Genotypes linked with bioactivities using multivariate analysis techniques. Antioxidants. 2022;11(6):1126. [CrossRef].
58. Einset J. Aneuploidy in relation to partial sterility in autotetraploid lettuce (*Lactuca sativa* L.). American J Botany. 1947;34(3):99–105. [CrossRef].
59. Trojak-Goluch A, Kawka-Lipińska M, Wielgusz K, Praczyk M. Polyploidy in industrial crops: Applications and perspectives in plant breeding. Agronomy. 2021;11(12):2574. [CrossRef].
60. Dolezel J. Plant DNA flow cytometry and estimation of nuclear genome size. Ann Bot. 2005;95(1):99–110. [CrossRef].
61. Ochatt SJ. Flow cytometry in plant breeding. Cytometry Pt A. 2008;73A(7):581–98. [CrossRef].
62. Dewitte A, Van K, Van J. Use of 2n gametes in plant breeding. In: Plant breeding. Vienna, Austria: InTech; 2012. [CrossRef].
63. Zhu B, Pan Q, Huo D, Zeng P, Cai B, Ge X, et al. Transcriptional aneuploidy responses of *Brassica rapa*-oleracea monosomic alien addition lines (MAALs) derived from natural allopolyploid *B. napus*. Front Genet. 2019;10:67. [CrossRef].
64. dos Reis GB, Ishii T, Fuchs J, Houben A, Davide LC. Tissue-specific genome instability in synthetic interspecific hybrids of *Pennisetum* purpureum (*Napier grass*) and *Pennisetum* glaucum (pearl millet) is caused by micronucleation. Chromosome Res. 2016;24(3):285–97. [CrossRef].

65. Xie L, Ke LZ, Lu XQ, Chen J, Zhang ZS. Exploiting unreduced gametes for improving ornamental plants. Front Plant Sci. 2022;13:883470. [CrossRef].
66. Devos KM, Sorrells ME, Anderson JA, Miller TE, Reader SM, Lukaszewski AJ, et al. Chromosome aberrations in wheat nullisomic-tetrasomic and ditelosomic lines. Cereal Res Commun. 1999;27(3):231–9. [CrossRef].
67. Gupta PK, Mir RR, Mohan A, Kumar J. Wheat genomics: Present status and future prospects. Int J Plant Genom. 2008;2008:896451. [CrossRef].